Solar RRL
www.solar-rrl.com

Optimizing SnO_2 Quantum Dot Precursor Solutions for Perovskite Solar Cells with Reduced Hysteresis

Gennaro V. Sannino, Thomas W. Gries, Qiong Wang, Maria Federica Caso, Antonella De Maria, Laura Lancellotti, Lucia V. Mercaldo, Ana Belén Muñoz-García, Michele Pavone, Antonio Abate, and Paola Delli Veneri**

In recent years, SnO_2 quantum dots (QDs) have been widely used for preparing the electron-transport layer within perovskite solar cells (PSCs). However, the fabricated devices exhibit an evident hysteresis unless interlayer materials are introduced to passivate or prevent the formation of trap states at the SnO_2–perovskite interface. Herein, the use of the zwitterion 3-(1-pyridinio)-1-propanesulfonate (PPS) as additive inside the SnO_2 QDs solution is proposed. The results highlight that the PPS plays a multifunctional role by accelerating the synthesis of the QDs, enhancing the electron transfer and passivating defects at the SnO_2–perovskite interface. The resulting PSCs with SnO_2 QDs incorporating PPS exhibit a remarkable reduction in hysteresis index (HI) compared to those prepared with thiourea or without any additives. This reduction in HI suggests that PPS serves as a cost-effective alternative additive for SnO_2 QDs preparation, eliminating the need for additional interlayers or expensive additives.

1. Introduction

In the last decade, perovskite solar cells (PSCs) have undoubtedly emerged as leaders in the field of next-generation solar cells. The excitement surrounding this technology has driven rapid advancements, and recently, a noteworthy 26.1%[1] in power conversion efficiency (PCE) has been achieved, equaling the record established for silicon homojunction solar cells. Although this rise in PCEs significantly slowed down in the last years,[2] there is still substantial room for further progress within PSCs. For instance, strategies for device stability issues, such as additive or interface engineering,[3,4] and the development of low-cost and scalable processes[5,6] are current topics in this field.

In a typical planar n–*i*–p PSC, the perovskite absorber is placed between two crucial components: the electron-transport layer (ETL) and the hole-transport layer. The primary role of the ETL is to transport electrons while preventing the passage of holes. Therefore, an effective ETL placed under the perovskite film must meet several criteria, including good level energy alignment, high carrier mobility, high optical transparency, and ease of manufacturing. However, there are additional considerations. Defects at the buried interface between the ETL and the perovskite layer can lead to perovskite degradation processes,[4,7,8] that severely threaten the stability of PSCs. Moreover, these defects also contribute to significant nonradiative recombination losses,[8–11] which affect the PCE and have an impact on the hysteresis behavior of the final device.[11–13] Hence, the morphology and surface wettability of the ETL are important features that play a significant role in influencing the quality of the perovskite film and the interface.[14,15]

Tin dioxide (SnO_2) is one of the most commonly used ETLs in PSCs, thanks to its exceptional properties that make it an excellent ETL candidate. Recent advances in deposition methods[16–20] and interface engineering strategies[8,16,21–25] have unlocked the full potential of this material, leading to PSCs achieving efficiencies exceeding 25%. As a result of its exceptional performance and its potential applications in flexible solar cells and tandem silicon perovskite devices, SnO_2 has finally outperformed titanium dioxide (TiO_2), which finds increasingly less usage within PSCs.

G. V. Sannino, M. F. Caso, A. De Maria, L. Lancellotti, L. V. Mercaldo, P. Delli Veneri
Italian National Agency for New Technologies
Energy and Sustainable Economic Development (ENEA)
80055 Portici (Na), Italy
E-mail: paola.delliveneri@enea.it

G. V. Sannino, M. Pavone
Department of Chemical Sciences
University of Naples Federico II
80126 Naples, Italy

T. W. Gries, Q. Wang, A. Abate
Department of Novel Materials and Interfaces for Photovoltaic Solar Cells
Helmholtz-Zentrum Berlin für Materialien und Energie GmbH
Berlin 14109, Germany
E-mail: antonio.abate@helmholtz-berlin.de

A. B. Muñoz-García
Department of Physics "E. Pancini"
University of Naples Federico II
80126 Naples, Italy

A. Abate
Department of Chemical Materials and Production Engineering
University of Naples Federico II
80125 Naples, Italy

The ORCID identification number(s) for the author(s) of this article can be found under https://doi.org/10.1002/solr.202300977.

DOI: 10.1002/solr.202300977

Solution-processed SnO_2 quantum dots (SnO_2 QDs) have received considerable attention due to the ease of manufacturing dense and uniform films, with wide bandgap (≈4.20 eV[26]), high reproducibility, and good performance. Yang et al.[19] used a simple method developed by Lu et al.[27] to prepare the SnO_2 QDs solution, in which the reactions of hydrolysis, dehydration, and oxidation were taken place in a solution of $SnCl_2{\cdot}2H_2O$ and distilled water in presence of thiourea (CH_4N_2S) as reaction accelerator and stabilizer. The SnO_2 layers obtained with this approach resulted in PSCs with a remarkable stabilized PCE of 20.32%. Successively, Liu et al.[28] removed the thiourea additive and performed the synthesis in a mixture of ethanol and deionized water to avoid residuals of additives in the film and reduce the cost and the temperature of the process. To further streamline the process, Xu et al.[29] developed a rapid microwave-assisted synthesis of SnO_2 QDs without adding any additives reducing considerably the time and cost. Recently, Luo et al.[15] investigated the difference in device performance between films obtained from SnO_2 nanoparticles and SnO_2 QDs solutions, demonstrating a higher performance for the latter. Nevertheless, in all the aforementioned studies, the fabricated PSCs exhibit a remarkable difference between reverse and forward scans, with hysteresis indexes (HI) ranging from 4.5% to over 20%.[15,19,28,29] This hysteretic behavior has been effectively mitigated through the use of ETL bilayer structures, reducing the charge accumulation capacitance at the buried interface, or with carbon-based interfacial layers, such as PCBM or C60-SAM, that can passivate or inhibit the formation of defects/trap states at the SnO_2–perovskite interface, such as oxygen vacancies, hydroxyl groups, and unsaturated coordinated metal atoms.[8] However, the introduction of these additional layers increases the complexity and cost of the PSC.

Ren et al.[18] introduced a novel approach for synthesizing SnO_2 QDs by incorporating the ligand 2-(2-aminoethyl) isothiourea dihydrobromide (2AT) as additive performing multiple functions. This ligand not only accelerates the synthesis reaction and stabilizes the QDs solution, but also plays a crucial role within the deposited SnO_2 film, passivating defects at the buried interface, improving the interfacial contact with the perovskite and regulating the perovskite crystallization. With the implementation of this approach, the researchers fabricated devices with a certified efficiency of 22.51% and negligible hysteresis without the use of any additional layer.

Herein, we propose the use of the zwitterion 3-(1-pyridinio)-1-propanesulfonate (PPS) as additive during the preparation of the SnO_2 QDs solution. This compound has already been employed in previous studies at the buried interface to form a chemical bridge, thereby enhancing device performance and stability. Choi et al.[30] introduced the PPS onto the SnO_2 ETL, passivating Pb–I antistite traps of the perovskite and forming interfacial dipoles that shifted the work function (WF) of the ETL and suppressed the interfacial charge recombination. More recently, Khan et al.[31] tested the PPS-covered SnO_2 within perovskite photodetectors, confirming a notable improvement in the interface and an enhanced charge extraction. Furthermore, Zhou et al.[24] observed its ability to form a chemical bridge and passivate defects of the perovskite also at the PTAA–perovskite interface. Therefore, we replaced the thiourea additive with PPS in SnO_2 QDs solutions, aspiring to enhance the characteristics of the ETL–perovskite interface.

Our results highlight that the PPS accelerates the synthesis of the QDs and stabilizes the solution. Besides, PPS plays an additional role at the SnO_2–perovskite interface enhancing the electron transfer and passivating defects. Fabricated PSCs reduced the HI from ≈8%, obtained with thiourea or without additives in the solution, to a value of ≈1%, using PPS. Our work suggests PPS as new effective additive alternative to thiourea for SnO_2 QDs preparation, obtaining devices with negligible hysteresis without the use of additional interlayers.

2. Results and Discussion

Two different types of additives, as illustrated in **Figure 1**, have been employed in the synthesis of SnO_2 QDs. Thiourea, used as reference, accelerates the reaction by consuming the HCl generated from hydrolysis processes. Additionally, thiourea bonds metal ions with its sulfur atom, surrounding the produced SnO_2 QDs with a positive charge generated by the protonated amino groups, which avoids the SnO_2 QDs aggregation. To replace thiourea, we have chosen to use PPS, a zwitterion composed of a sulfonate group (SO_3^-) and a pyridine ring. Similarly, the synthesis of QDs is accelerated by HCl consumption in this case as well. PPS interacts with Sn by forming bonds with the sulfonate group,[31,32] consequently inhibiting the aggregation of QDs with the surrounding positive pyridine rings. Moreover, experimental evidences demonstrate that PPS offers additional benefits within a PSC. It can enhance interface quality by forming coordination bonds with Pb^{2+}, or it can passivate perovskite defects, such as halide vacancies and lead-halide antisites.[24,31]

We synthesized SnO_2 QDs using 0.7 or 0.1 molar ratios of PPS to $SnCl_2{\cdot}2H_2O$, terminating the process after 1 and 2 days, respectively. The varying concentration of PPS directly influences the conversion time of the solution, illustrating the accelerating role of PPS in the synthesis reaction. Dynamic light scattering (DLS) measurements of the resulting solutions (**Figure 2**a) revealed a peak at approximately 13 nm, indicating a homogenous population of SnO_2 QDs. At higher size values, another peak is visible (Figure S1a, Supporting Information), more pronounced in the solution containing the higher concentration of PPS and barely visible in the other. We attribute this additional peak to the excess of PPS.

The corresponding SnO_2 films, deposited via spin coating, evinced thicknesses of 15 and 100 nm for the low and high PPS molar ratio solutions, respectively. The presence of a

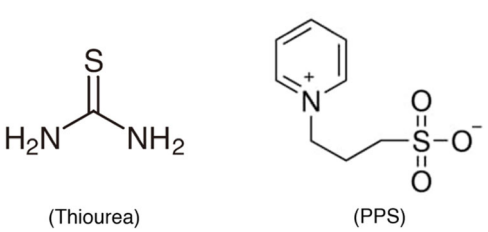

Figure 1. Thiourea and PPS used as additives in the synthesis of the SnO_2 QDs.

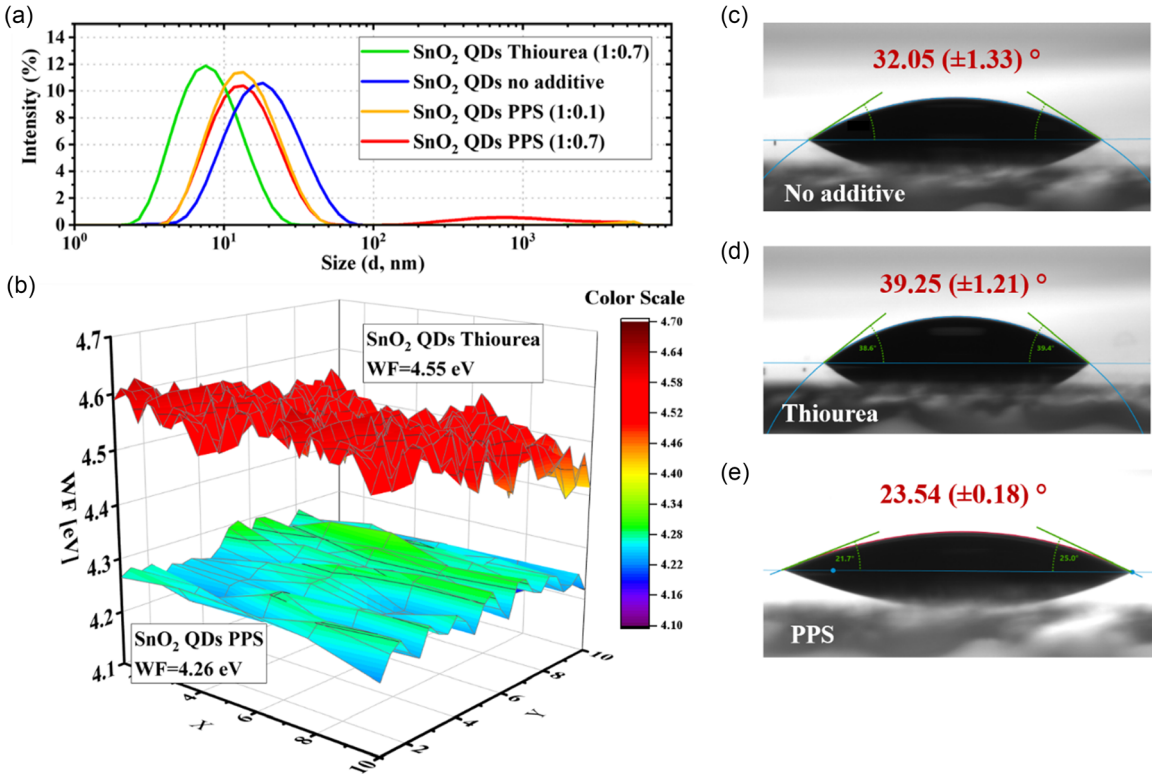

Figure 2. a) DLS measurements performed on SnO_2 QDs solutions without additive (blue), with 0.7 molar ratio of thiourea (green) or PPS (red) to $SnCl_2{\cdot}2H_2O$, and 0.1 (orange) molar ratio of PPS to $SnCl_2{\cdot}2H_2O$; b) 2D WF maps for SnO_2 thiourea and SnO_2 PPS films; pictures of contact angle measurements of c) no additive, d) thiourea, and e) PPS SnO_2 films with water as the liquid.

significant excess of PPS in the solution leads to the higher thickness. As shown in Figure S1b, Supporting Information, the film changes to an opaque appearance after a few days, likely due to PPS exposure to the air. Consequently, we continued our investigation using the weakly concentrated PPS solution.

To verify the actual impact of the PPS additive, we have compared the results with both a SnO_2 QDs solution obtained using thiourea as additive and one without any additives. DLS investigation has confirmed a homogeneous QDs population in all precursor solutions (Figure 2a). Specifically, peaks are observed at the following size values: 7.5 nm (thiourea) <13 nm (PPS) <17 nm (no additive). The observed hydrodynamic radii align with the defined range for QDs (1–10 nm).[33] As additional evidence confirming the quantum nature of the particles, we performed DLS measurements on the commercial Alfa-Aesar solution containing SnO_2 nanoparticles (Figure S1c, Supporting Information), revealing a heterogeneous population with a peak at a higher order of magnitude (≈120 nm). Solutions containing additives also exhibit a weak peak at higher size values (Figure S1a, Supporting Information) absent in the additive-free solution. This observation confirms that the peak is attributed to the presence of the additive.

Figure 2b shows the results obtained from Kelvin probe measurements on deposited films. The SnO_2 PPS film exhibits a lower WF of 4.26 eV respect to the SnO_2 thiourea film (4.55 eV). Choi et al.[30] observed a slight shift in the WF caused by the presence of PPS deposited on top of SnO_2, attributed to the dipole effects of the zwitterionic molecule. Kelvin probe results confirm the presence of PPS within the film and demonstrate that PPS affects the surface properties of the deposited film, even when used as an additive in the SnO_2 QDs solution.

Additional evidence supporting the existence of the PPS additive within the film is provided through contact angle measurements, as shown in Figure 2c–e. The SnO_2 PPS film exhibits the lowest contact angle, indicating a high hydrophilicity of the surface, as expected with the presence of the PPS zwitterion.

Variation in the thickness of the different SnO_2 films, attributed to the additives molecules within the deposited films, are also revealed from UV–vis spectroscopy and ellipsometry measurements (Figure S2a–c, Supporting Information). In particular, from ellipsometry thicknesses of approximately 9 nm for films without additives, 12 nm for those with thiourea, and 14 nm for films with PPS have been evaluated.

Subsequently, we fabricated devices using these three SnO_2 QDs films. **Figure 3**a displays the architecture of the PSC, while **Figure** 3b–d and **4** present the *J–V* curves and statistical box charts of the photovoltaic (PV) parameters, respectively. While the QDs film type does not affect significantly the overall device performance, it is noteworthy that the PSCs employing SnO_2 PPS exhibit a relevant reduction of the hysteresis in the *J–V* scans, with improved FF in forward scan direction. **Figure 5** presents the calculated HI for a quantification of the effect, showing that the hysteresis issue is practically solved when employing

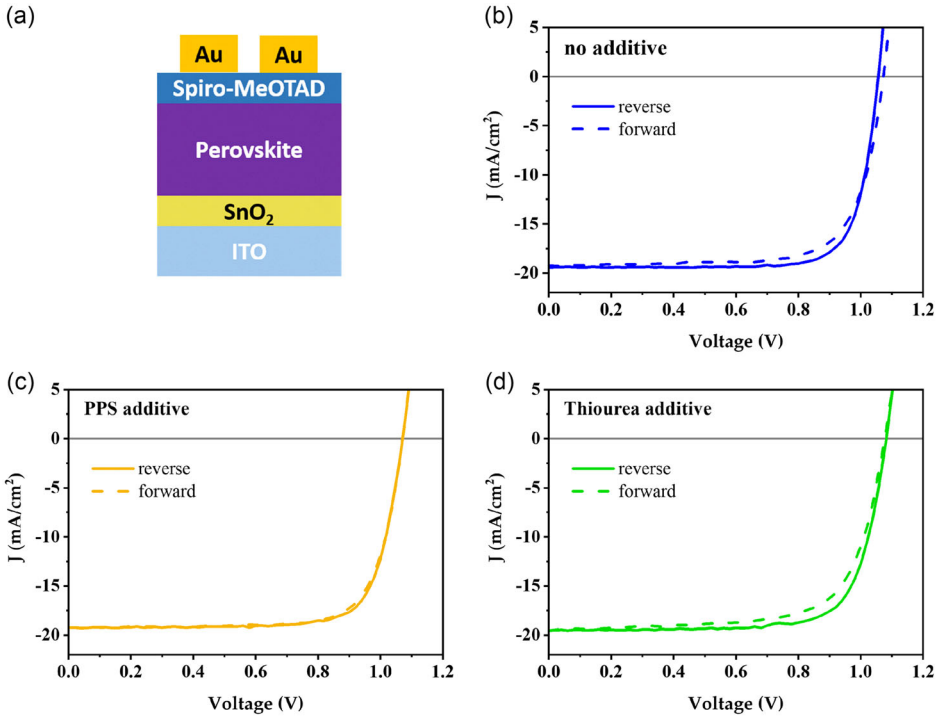

Figure 3. a) PSC configuration used to test the SnO_2 QD-based ETLs; b–d) reverse and forward *J–V* curves depicted, respectively, with solid and dashed lines of devices with different SnO_2 QDs film as ETL.

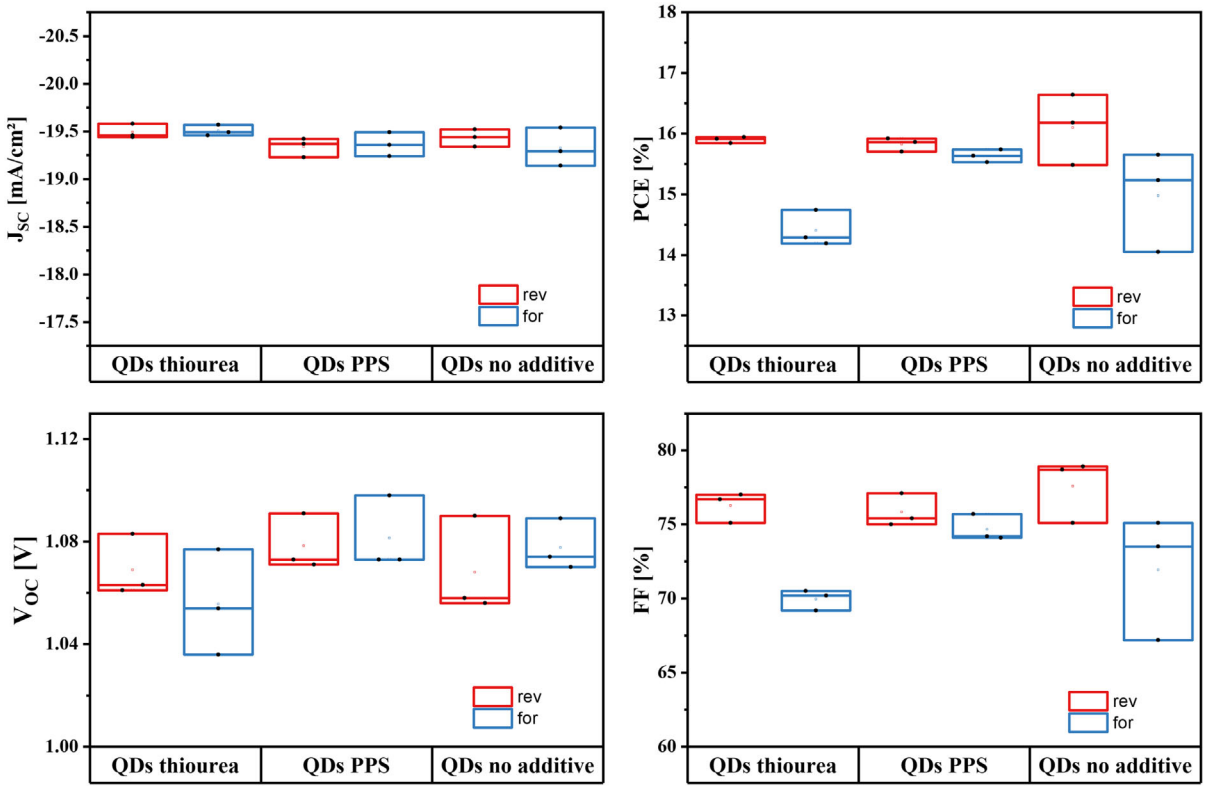

Figure 4. Statistical box charts of the PV parameters extracted from devices with different SnO_2 QDs as ETL.

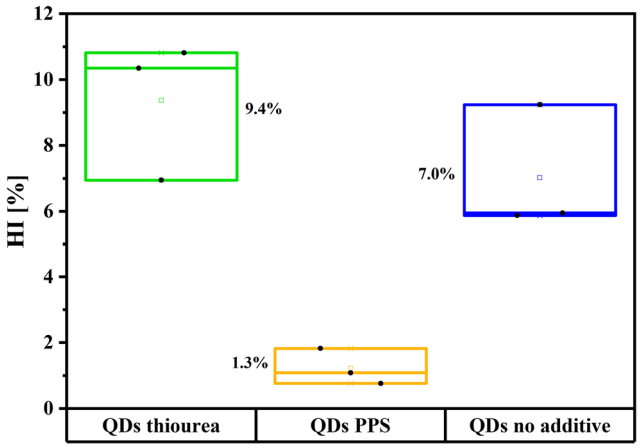

Figure 5. Statistical box chart of the HI extracted from devices with different SnO_2 QDs as ETL.

SnO_2 PPS. There is also a possible slight enhancement of the V_{OC} parameter (a few mV) in this case (Figure 4), to be confirmed with further investigation. At the same time, the short-circuit current density is essentially unchanged, as also validated by the external quantum efficiency (EQE) spectra (Figure S3, Supporting Information). In particular, the spectral shape at low λ does not evidence significant effects stemming from possibly different parasitic optical losses of the tested QD films, as expected from UV–vis spectroscopy and ellipsometry results.

This decreased hysteresis has been previously observed in PSCs utilizing PPS as interlayer between the charge-transport layer and the perovskite.[24,30] Theoretical calculations have demonstrated the passivation of perovskite trap states through the interaction between the positively charged atoms in the PPS zwitterion and perovskite Pb–I antisite defects.[30] It is well known that defects passivation at the interface reduces hysteresis phenomena within the PSC.[12,34] The obtained results from WF measurements and contact angle analysis clearly indicate the presence of PPS molecules on the surface of films deposited from SnO_2 QDs PPS solutions. Therefore, the reduction in hysteresis confirms that the beneficial effects induced by PPS as interlayer are effective even when PPS serves as additive in the SnO_2 QDs precursor solution. PPS binds to the SnO_2 with the sulfonate group, passivating perovskite defects with the pyridine ring. Moreover, these interactions enhance the interfacial contact between the two materials and generate a dipole at the interface pointing toward the SnO_2 film, decreasing the WF of the pristine SnO_2 and further increasing the ETL performance.[35] Thus, the reduction in hysteresis is likely a consequence of various factors, including a more favorable band energy alignment due to PPS dipole effects, defects passivation, and the formation of a chemical bridge between the SnO_2 film and the perovskite, which could facilitate the electron transport from the perovskite to the SnO_2 layer.

3. Conclusions

Our study explores the use of PPS as an additive in the synthesis of SnO_2 QDs for applications in PSCs. Building upon the success of PPS in previous studies at the buried interface, our results demonstrate that PPS accelerates QD synthesis, stabilizes the solution, and enhances electron transfer at the SnO_2–perovskite interface. The fabricated PSCs using SnO_2 QDs with PPS exhibit a significant reduction in HI compared to those prepared with thiourea or without additives. The improvement in HI suggests that PPS serves as an effective and cheap alternative additive for SnO_2 QDs preparation, eliminating the need for additional interlayers or expensive additives as 2AT. Our findings contribute to the ongoing efforts to reduce the number of processes involved in the fabrication of a PSC and simplify their application to facilitate large-scale production of PSCs.

4. Experimental Section

Materials: Formamidinium iodide (FAI), methylammonium bromide (MABr), $SnCl_2{\cdot}2H_2O \geq 99.99\%$, thiourea $\geq$99.0%, PPS, Spiro-MeOTAD99%, lithium bis(trifluoromethanesulfonyl)imide salt (Li-TFSI), 4-*tert*-butylpyridine (*t*-BPY), FK209 Co (III) TFSI salt, and all the solvents were purchased from Sigma–Aldrich. CsI 99.999% was obtained from ACROS Organics. $PbBr_2$ 99.998% was purchased from Alfa-Aesar. PbI_2 99.99% was purchased from TCI Europe. ITO-covered glass substrates (10 Ω sq^{-1}) were purchased from Kintec.

Device Fabrication and Characterization: The ITO substrates were cleaned by sonicating in a 2% Mucasol deionized water solution, acetone, and finally IPA for 15 min each. The SnO_2 QDs solutions were prepared by adding $SnCl_2$ dihydrate powder (0.15 M) to a continuously stirred solution of deionized water, containing an additive or left pristine. In particular, the molar concentration used for the thiourea and PPS additives was, respectively, 0.10 and 0.015 M. The bottle was left opened to expose the solution directly to air. It took approximately 1 and 2 days, respectively, for the thiourea solution and the PPS or pure solution to complete the synthesis of the QDs. This process changed the initially milky solution, due to the fast formation of hydrolysis products, into a clear and yellow solution. The concentration of the solutions was restored to 0.15 M by adding an adequate amount of deionized water. The obtained SnO_2 QDs solutions were filtered using a 0.22 µm PTFE filter and stored at 2–5 °C before use. Prior to depositing the SnO_2 film, the ITO substrates were treated with UV–ozone for 25 min. SnO_2 QDs solutions, previously filtered using a 0.22 µm PTFE filter, were deposited in air with the spin-coating technique at 3000 rpm, reached in 3 s, for 30 s. Then, the deposited films were annealed on a hot plate for 1 h at 150 °C. The triple-cation and double-anion perovskite ($Cs_{0.05}(FA_{0.83}MA_{0.17})_{0.95}Pb(I_{0.83}Br_{0.17})_3$ with 9% PbI_2 excess) was deposited via one-step antisolvent process in a nitrogen-filled glove box. In particular, a precursor solution containing FAI (1.00 M), PbI_2 (1.09 M), MABr (0.20 M), and $PbBr_2$ (0.20 M) in DMF/DMSO (4:1 v/v%) was spun on top of SnO_2 films pretreated with UV–ozone for 25 min. The deposition process consists of two spin-coating steps: the first at 1000 rpm (200 rpm s^{-1}) for 10 s and a second at 6000 rpm (2000 rpm s^{-1}) for 20 s. During the second step, 150 µL of CBZ was spun in one shot on top of the substrates 2 s before the end of the spinning program. The light brown films were then annealed at 100 °C for 1 h, obtaining dark brown perovskite films. A 0.060 M Spiro-MeOTAD solution in CBZ was prepared doping 1 mL with 17 µL of a 1.8 M Li-TFSI stock solution in ACN, 27 µL of *t*-BPY, and 7 µL of a 0.25 M FK 209 Co(III) TFSI stock solution in ACN. The corresponding film was deposited via spin coating at 4000 rpm for 30 s in a nitrogen-filled glove box. Finally, a 80 nm thick Au electrode was deposited via thermal evaporation.

DLS measurements were performed with a Zetasizer Nano ZS He–Ne laser 633 nm, 4 mW. WFs were evaluated using the SKP5050 Scanning Kelvin Probe. Optical properties were investigated using spectroscopic ellipsometry (VASE ellipsometer) and UV–vis spectroscopy (PerkinElmer λ-900 spectrophotometer). The static water contact angle was measured with the direct optical method of drop-shape analysis, by means of the contact angle meter KRUSS DSA-100. Solar cells were

characterized in ambient air by measuring the illuminated current–voltage (*J–V*) characteristic at AM1.5G under a class A Xenon lamp SpectroSun X25 Mark II solar simulator. *J–V* data were acquired with a scan rate of 100 mV s^{-1}. The irradiated area was 0.1 cm^2, defined by applying a shadow mask. The EQE was measured with a Bentham PVE300 setup in DC mode. Integrated J_{SC} from EQE spectra was in agreement (within 0.5 mA cm^{-2}) with values extracted from *J–V* curves.[36]

Supporting Information

Supporting Information is available from the Wiley Online Library or from the author.

Acknowledgements

This research was funded by MASE (Ministero dell'Ambiente e della Sicurezza Energetica) in the framework of the Operating Agreements with ENEA for Mission Innovation and Research on the Electric System.

Conflict of Interest

The authors declare no conflict of interest.

Data Availability Statement

The data that support the findings of this study are available on request from the corresponding author. The data are not publicly available due to privacy or ethical restrictions.

Keywords

electron-transport layers, hysteresis, perovskite solar cells, quantum dots, SnO_2

Received: November 28, 2023
Revised: January 8, 2024
Published online: February 12, 2024

[1] Best research-cell efficiencies NREL **2023**. https://www.nrel.gov/pv/cell-efficiency.html (accessed: November 2023).
[2] G. Szabó, N.-G. Park, F. De Angelis, P. V. Kamat, *ACS Energy Lett.* **2023**, *8*, 3829.
[3] T. A. Chowdhury, M. A. Bin Zafar, M. Sajjad-Ul Islam, M. Shahinuzzaman, M. A. Islam, M. U. Khandaker, *RSC Adv.* **2023**, *13*, 1787.
[4] L. Duan, A. Uddin, *Mater. Chem. Front.* **2022**, *6*, 400.
[5] S. H. Reddy, F. Di Giacomo, A. Di Carlo, *Adv. Energy Mater.* **2022**, *12*, 2103534.
[6] H. Yin, P. Lv, B. Gao, Y. Zhang, Y. Zhu, M. Hu, B. Tan, M. Xu, F. Huang, Y.-B. Cheng, A. N. Simonov, J. Lu, *J. Mater. Chem. A* **2022**, *10*, 25652.
[7] J. Wu, J. Shi, Y. Li, H. Li, H. Wu, Y. Luo, D. Li, Q. Meng, *Adv. Energy Mater.* **2019**, *9*, 1901352.
[8] Z.-W. Gao, Y. Wang, W. C. H. Choy, *Adv. Energy Mater.* **2022**, *12*, 2104030.
[9] D. Luo, X. Li, A. Dumont, H. Yu, Z.-H. Lu, *Adv. Mater.* **2021**, *33*, 2006004.
[10] B. Li, Y. Xiang, K. D. G. I. Jayawardena, D. Luo, Z. Wang, X. Yang, J. F. Watts, S. Hinder, M. T. Sajjad, T. Webb, H. Luo, I. Marko, H. Li, S. A. J. Thomson, R. Zhu, G. Shao, S. J. Sweeney, S. R. P. Silva, W. Zhang, *Nano Energy* **2020**, *78*, 105249.
[11] E. Aydin, M. De Bastiani, S. De Wolf, *Adv. Mater.* **2019**, *31*, 1900428.
[12] D.-H. Kang, N.-G. Park, *Adv. Mater.* **2019**, *31*, 1805214.
[13] H. Yu, H. Lu, F. Xie, S. Zhou, N. Zhao, *Adv. Funct. Mater.* **2016**, *26*, 1411.
[14] S. Foo, M. Thambidurai, P. Senthil Kumar, R. Yuvakkumar, Y. Huang, C. Dang, *Int. J. Energy Res.* **2022**, *46*, 21441.
[15] Z. Luo, G. Du, L. Yang, J. Zhang, *J. Power Sources* **2023**, *568*, 232928.
[16] S. Y. Park, K. Zhu, *Adv. Mater.* **2022**, *34*, 2110438.
[17] J. J. Yoo, G. Seo, M. R. Chua, T. G. Park, Y. Lu, F. Rotermund, Y.-K. Kim, C. S. Moon, N. J. Jeon, J.-P. Correa-Baena, V. Bulović, S. S. Shin, M. G. Bawendi, J. Seo, *Nature* **2021**, *590*, 587.
[18] Z. Ren, K. Liu, H. Hu, X. Guo, Y. Gao, P. W. K. Fong, Q. Liang, H. Tang, J. Huang, H. Zhang, M. Qin, L. Cui, H. T. Chandran, D. Shen, M.-F. Lo, A. Ng, C. Surya, M. Shao, C.-S. Lee, X. Lu, F. Laquai, Y. Zhu, G. Li, *Light Sci. Appl.* **2021**, *10*, 239.
[19] G. Yang, C. Chen, F. Yao, Z. Chen, Q. Zhang, X. Zheng, J. Ma, H. Lei, P. Qin, L. Xiong, W. Ke, G. Li, Y. Yan, G. Fang, *Adv. Mater.* **2018**, *30*, 1706023.
[20] S.-U. Lee, H. Park, H. Shin, N.-G. Park, *Nanoscale* **2023**, *15*, 5044.
[21] H. Min, D. Y. Lee, J. Kim, G. Kim, K. S. Lee, J. Kim, M. J. Paik, Y. K. Kim, K. S. Kim, M. G. Kim, T. J. Shin, S. Il Seok, *Nature* **2021**, *598*, 444.
[22] E. Wang, P. Chen, X. Yin, Y. Wu, W. Que, *Sol. RRL* **2019**, *3*, 1900041.
[23] G. V. Sannino, A. Pecoraro, P. Maddalena, A. Bruno, P. D. Veneri, M. Pavone, A. B. Muñoz-García, *Sustainable Energy Fuels* **2023**, *7*, 4855.
[24] Q. Zhou, J. Qiu, Y. Wang, M. Yu, J. Liu, X. Zhang, *ACS Energy Lett.* **2021**, *6*, 1596.
[25] G. V. Sannino, A. De Maria, V. La Ferrara, G. Rametta, L. V. Mercaldo, M. L. Addonizio, L. Lancellotti, A. Pecoraro, A. B. Muñoz-García, M. Pavone, P. Delli Veneri, *Solids* **2021**, *2*, 407.
[26] M. S. Kiani, Z. T. Sadirkhanov, A. G. Kakimov, H. P. Parkhomenko, A. Ng, A. N. Jumabekov, *Nanomaterials* **2022**, *12*, 2615.
[27] X. Lu, H. Wang, Z. Wang, Y. Jiang, D. Cao, G. Yang, *J. Alloys Compd.* **2016**, *680*, 109.
[28] H. Liu, Z. Chen, H. Wang, F. Ye, J. Ma, X. Zheng, P. Gui, L. Xiong, J. Wen, G. Fang, *J. Mater. Chem. A* **2019**, *7*, 10636.
[29] Z. Xu, Y. Jiang, Z. Li, C. Chen, X. Kong, Y. Chen, G. Zhou, J.-M. Liu, K. Kempa, J. Gao, *ACS Appl. Energy Mater.* **2021**, *4*, 1887.
[30] K. Choi, J. Lee, H. I. Kim, C. W. Park, G.-W. Kim, H. Choi, S. Park, S. A. Park, T. Park, *Energy Environ. Sci.* **2018**, *11*, 3238.
[31] A. A. Khan, N. Kumar, U. Jung, W. Heo, Z. Tan, J. Park, *Nanoscale Horiz.* **2023**, *8*, 1577.
[32] D. Zheng, R. Peng, G. Wang, J. L. Logsdon, B. Wang, X. Hu, Y. Chen, V. P. Dravid, M. R. Wasielewski, J. Yu, W. Huang, Z. Ge, T. J. Marks, A. Facchetti, *Adv. Mater.* **2019**, *31*, 1903239.
[33] D. Chen, S. Huang, R. Huang, Q. Zhang, T.-T. Le, E. Cheng, Z. Hu, Z. Chen, *Mater. Res. Lett.* **2018**, *6*, 462.
[34] S. Srivastava, S. Ranjan, L. Yadav, T. Sharma, S. Choudhary, D. Agarwal, A. Singh, S. Satapathi, R. K. Gupta, A. Garg, K. S. Nalwa, *Commun. Mater.* **2023**, *4*, 52.
[35] Q. Chen, C. Wang, Y. Li, L. Chen, *J. Am. Chem. Soc.* **2020**, *142*, 18281.
[36] L. V. Mercaldo, E. Bobeico, A. De Maria, M. Della Noce, M. Ferrara, L. Lancellotti, A. Romano, G. V. Sannino, G. Nasti, A. Abate, P. Delli Veneri, *Energy Technol.* **2022**, *10*, 2200748.